

TITLE

ASP Conference Series, Vol. **VOLUME**, **PUBLICATION YEAR**

EDITORS

Cluster cores as observed with Chandra

S. Ettori and A.C. Fabian

Institute of Astronomy, Madingley Road, CB3 0HA Cambridge

Abstract. We review recent results from Chandra observations of the X-ray bright cores of clusters of galaxies. We discuss the detection of "cold fronts" and their implication for thermal conduction, the interaction of cooling flow and radio source in the Perseus cluster and the dynamical state of the central region of A1795. The radial distribution of metals in A1795 and the azimuthal variation in metallicity in 4C+55.16 are presented.

1. Introduction

At radii of few hundred kpc, the intracluster medium (ICM) has a characteristic density $n_{\text{gas}} \sim 10^{-3} \text{ cm}^{-3}$, temperature $T_{\text{gas}} \sim 10^8 \text{ K}$ and a heavy element abundance of about 40 per cent of the solar value. The density drops at larger radii approximately as r^{-2} . Hence, under these conditions, the gas appears as an optically thin plasma in ionization equilibrium emitting X-rays, where the ionization and emission processes result mainly from collisions of ions with electrons. This emission is mostly due to thermal bremsstrahlung (free-free emission) when $T_{\text{gas}} > 3 \times 10^7 \text{ K}$, with an emissivity $\propto n_{\text{gas}}^2 T_{\text{gas}}^{1/2}$. In the core, where the density is higher, a larger amount of energy is radiated away and cooling takes place on timescale

$$t_{\text{cool}} = 1.4 \times 10^8 \frac{kT_{\text{gas}}}{2 \text{ keV}}^{0.5} \frac{n_{\text{gas}}}{0.1 \text{ cm}^{-3}}^{-1} \text{ yrs} < t_{\text{age}} \approx t_{\text{Hubble}} \quad (1)$$

This inequality is satisfied in the core of about 70 per cent of nearby clusters (Peres et al. 1998), like A1795 (Fig. 1). The drops in temperature and the small cooling time suggest that a subsonic flow of gas moves inward in the hydrostatic core atmosphere under the influence of gravity and the weight of overlying plasma (see Fabian 1994 for a review on this cooling flow scenario). The inferred deposition rates range from $< 10 M_{\odot} \text{ yr}^{-1}$ in poor clusters to $> 1000 M_{\odot} \text{ yr}^{-1}$ in massive systems. However, only 10 per cent of these cooling rates can be accounted for from normal star formation (see Crawford et al. 1999 and references therein).

Here we review some recent results from Chandra observations of the cluster central regions on (i) the physical condition of the plasma and (ii) how the metals are distributed and the gas enrichment is produced.

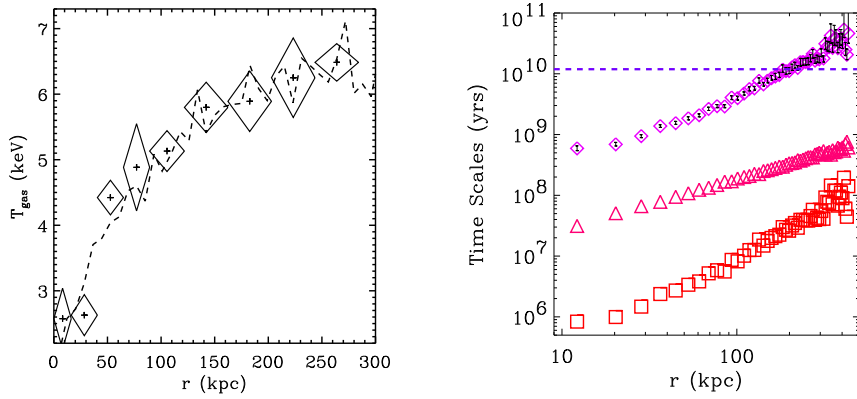


Figure 1. Chandra observation of A1795. (Left) Temperature profile from both spatial (i.e. inverting the surface brightness given an assumed potential law and the hydrostatic equilibrium; dashed line) and spectral (i.e. directly from spectral fitting; diamonds) deprojection analyses (Ettori et al. 2001). (Right) The cooling time, t_{cool} (diamonds), the sound crossing time (triangles) and the equipartition time by Coulomb collisions (squares) are compared to the age of the Universe (dashed line; $H_0 = 50 \text{ km s}^{-1} \text{ Mpc}^{-1}$, $\Omega_m = 1$).

2. Cold fronts and thermal conduction in cluster cores

The Chandra observations of "cold fronts" in some clusters (e.g. A2142, Markevitch et al. 2000; A3667, Vikhlinin, Markevitch, & Murray 2001; RX J1720+2638, Mazzotta et al. 2001), where regions of plasma with differences in temperature by a factor of 2 lie close to each other, allow a direct constraint on the efficiency of the thermal conduction (Ettori & Fabian 2000).

The heat stored in the intracluster plasma is conducted down any temperature gradient present in the gas in a way that can be described through the following equations (Spitzer 1962, Sarazin 1988):

$$q = -\frac{d(kT_e)}{dr}; \quad (2)$$

where q is the heat flux, T_e is the electron temperature, and κ is the thermal conductivity that can be expressed in terms of the density, n_e , the electron mass, m_e , and the electron mean free path, $\lambda_e = 30.2 \frac{kT_e}{10 \text{ keV}}^2 \frac{n_e}{10^{-3} \text{ cm}^{-3}}^{-1} \text{ kpc}$, as (Cowie and McKee 1977) $\kappa = 1.31 n_e m_e (kT_e/m_e)^{1/2} = 8.2 \cdot 10^{20} (kT_e/10 \text{ keV})^{5/2} \text{ erg s}^{-1} \text{ cm}^{-1} \text{ keV}^{-1}$.

The maximum heat flux in a plasma is given by $q = \frac{3}{2} n_e kT_e v$, where $v = dr/dt$ is a characteristic velocity that we are now able to constrain equalizing the latter equation to eqn. 2.

From the observed plasma properties in A2142 (Fig. 2), we note that the temperature varies by a factor of 2 on a scale length of about 10–15 kpc. These

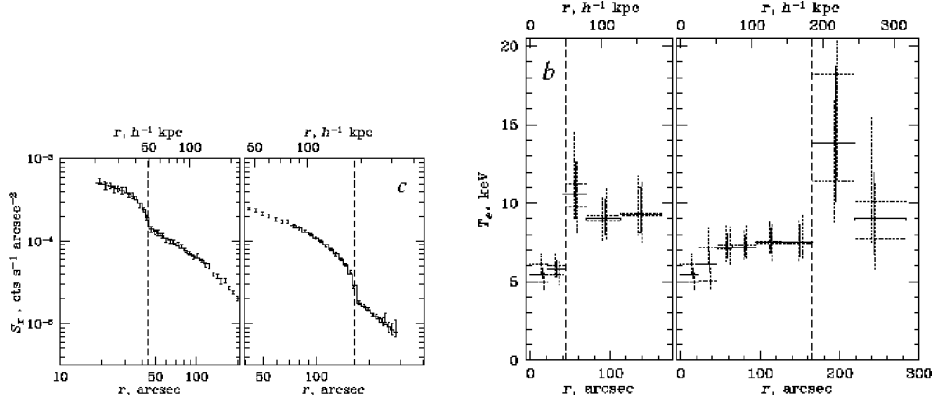


Figure 2. (Left) Surface brightness profiles across the two edges in A2142. (Right) Temperature profiles along the same sectors. (From Markevitch et al. 2000).

value imply that the characteristic time, τ_{cond} , required to erase the electron temperature gradient and due to the action of the thermal conduction alone would be few times 10^6 years. When this time interval is compared with either the core crossing time of the interacting clumps of about 10^9 yrs or a dynamical timescale of about $> 2 \times 10^7$ yrs from the model suggested by Markevitch et al., we conclude that thermal conduction needs to be suppressed by a factor larger than 10 and with a minimum characteristic value enclosed between 250 and 2500. The frequency of the occurrence of similar structures in other cluster cores will be important in establishing the timescale for their formation and duration and, hence, improve the constraint on the thermal conduction in the intracluster plasma.

This result is a direct measurement of a physical process in the ICM and implies that thermal conduction is particularly inefficient within $280 h_{70}^{-1}$ kpc of the central core. The observed sharp temperature boundaries also mean that mixing and diffusion are minimal. The gas in the central regions of many clusters has a cooling time lower than the overall age of the system, so that a slow flow of hotter plasma moves here from the outer parts to maintain hydrostatic equilibrium. In such a cooling flow (e.g. Fabian 1994), several phases of the gas (i.e. with different temperatures and densities) are in equilibrium and would thermalize if the conduction time were short. The large suppression of plasma conductivity in the cluster core allows an inhomogeneous, multi-phase cooling flow to form and be maintained, as is found from spatial and spectral X-ray analyses of many clusters (e.g. Allen et al. 2001).

3. Interaction of radio source and cooling flow in the Perseus cluster

The Perseus cluster (Abell 426) at a redshift of 0.0183 is the brightest cluster in the X-ray sky. A radio source, 3C 84, is powered at the centre of the central galaxy, NGC 1275 (Fig. 3). The Chandra X-ray observatory observed its core for about 24 ksec (Fabian et al. 2000). X-ray colours can be obtained to reconstruct

the temperature and absorption maps. The temperature map (Fig. 3) shows that the gas is cooler towards the centre and, in particular, the coolest one lies along the rims of the inner radio lobes. From the surface brightness we can obtain the gas density and, thus, radiative cooling time that appears shortest in the very central regions. There is no evidence for heating due to the radio source beyond the lobes, that are probably cleared of cooler gas. No sign of strong shocks is present.

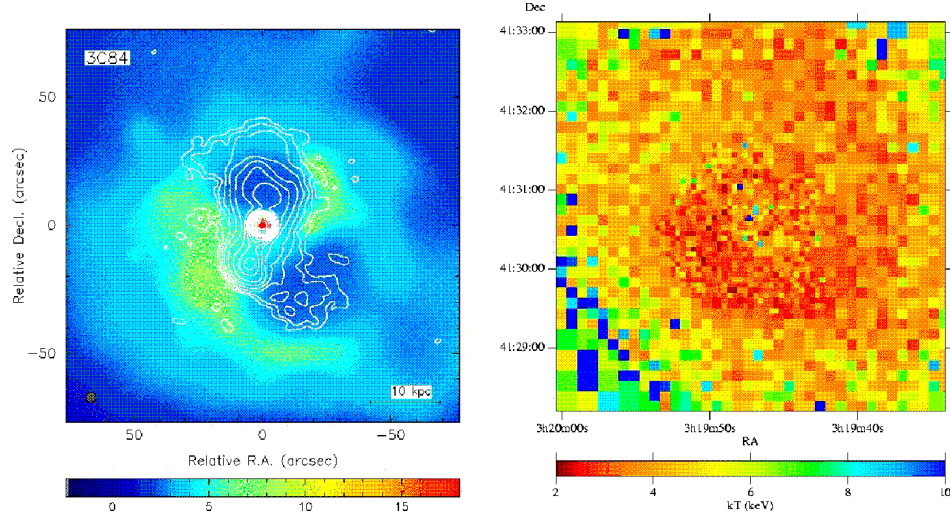


Figure 3. (Left) Radio image (1.4 GHz restored with a 5 arcsec beam; produced by G. Taylor) overlaid on adaptively smoothed 0.5–7 keV X-ray map. (Right) Temperature map of the core of the Perseus cluster obtained from X-ray color ratios (Fabian et al. 2000). Note that the coolest gas ($T \approx 2.5$ keV) with a cooling time of about 0.3 Gyr lies in the rim around the lobes to the North and East.

4. Dynamical state of the core of A 1795

Abell 1795 is a nearby ($z = 0.063$) rich CD galaxy cluster well studied at optical, radio and X-ray wavelengths. It has been observed for 18.4+19.4 ksec from Chandra (Fabian et al. 2001b, Ettori et al. 2001; Fig. 4).

To constrain the physical quantities of the ICM, we apply the deprojection analysis, assuming that the X-ray is spherically symmetric and the plasma is in hydrostatic equilibrium with the underlying gravitational potential (cf. Fig. 1). In our spectral analysis, we are able to resolve in 5 radial bins the gas temperature profile in the inner 100 kpc radius with a relative uncertainty less than 5 (10) per cent for the projected (deprojected) temperature. The electron density is estimated from the spectral best-fit results. Then, we apply directly the equation of hydrostatic equilibrium between the gravitational potential and the intracluster plasma to estimate the mass profile, $M_X(<r)$ (Fig. 5).

In particular, we can investigate the slope of a power law expression of the dark matter profile, $\rho_{\text{grav}} = \rho_0(r=r_0)^{-\alpha}$, that is a proper approximation for

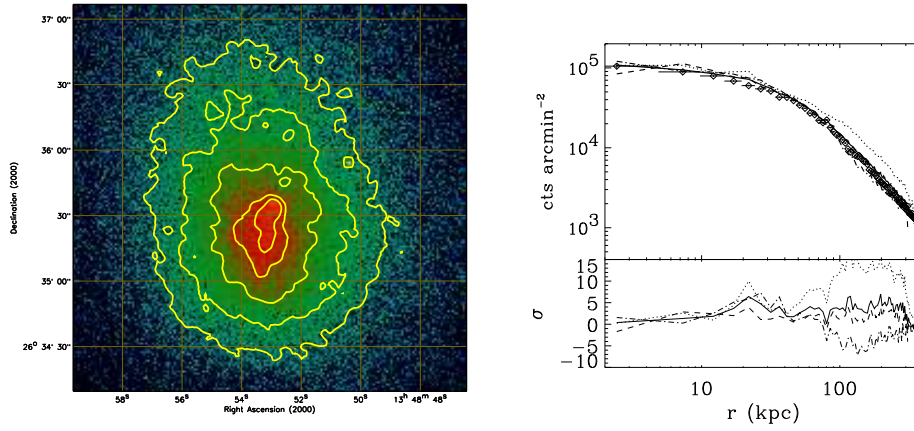


Figure 4. (Left) Smoothed image of the Chandra observation of A1795. In the centre, it is evident an elongated feature with the cD galaxy corresponding to the bump in brightness to the North (Fabian et al. 2001b). (Right) Brightness profiles extracted from four sectors (x axis at 0°, y axis at 90°): 50°–135° (‘‘Northern excess’’, dotted line), 135°–170° (dashed line), 170°–270° (‘‘Southern deficit’’, dot-dashed line), 270°–50° (diamonds). The azimuthally averaged profile is represented with a solid line. The residuals are plotted with respect to the 270°–50° profile. Note that, starting at about 50 kpc, the excess in the North-East and the deficit in the South-East become evident with deviations respective to the West region of about 10%.

the inner part of the cluster potential, integrating it over the volume ($M_{\text{grav}}(< R) = \int_0^R 4\pi \rho_{\text{grav}} r^2 dr / R^3$) and fitting the obtained mass profile to the one observed (Fig. 5) between 10 and 100 kpc, where the discrepancy among the different models is more significant. We measure $\beta = 0.59^{+0.12}_{-0.17}$ (1 σ ; in the range 0.27–0.81 at the 90 per cent confidence level), that indicates a remarkable flat profile suggesting the presence of a core.

The surface brightness distribution (Fig. 4) suggests that the intracluster medium has an unrelaxed nature that might introduce a kinetic pressure component in the hydrostatic equilibrium equation so raising the total effective mass in the central core. This could possibly explain the flattening of the gravitating mass profile. Assuming that underlying potential is described from the potential in Navarro et al. (1997) and ΔM is the difference with respect to the observed mass estimates, a bulk motion with velocity (assumed independent from radial position) of 300 km s^{-1} is required from the equation $d(v_{\text{gas}}^2)/dr = -(G_{\text{gas}} + \Delta M)/r^2$. This value is lower than the gas sound speed of about 800 km s^{-1} and definitely subsonic. The shape of the gravitational potential is also consistent with the detected motion of the cD galaxy. Oegerle & Hill (1994) measure a cD velocity redshifted relative to the cluster of 150 km s^{-1} . The emission-line velocity map in Hu, Cowie, & Wang (1985) shows that the H α /X-ray filament has the same velocity of the cluster and is blueshifted from the cD velocity by still 150 km s^{-1} . In Fig. 5, the cD velocity is estimated

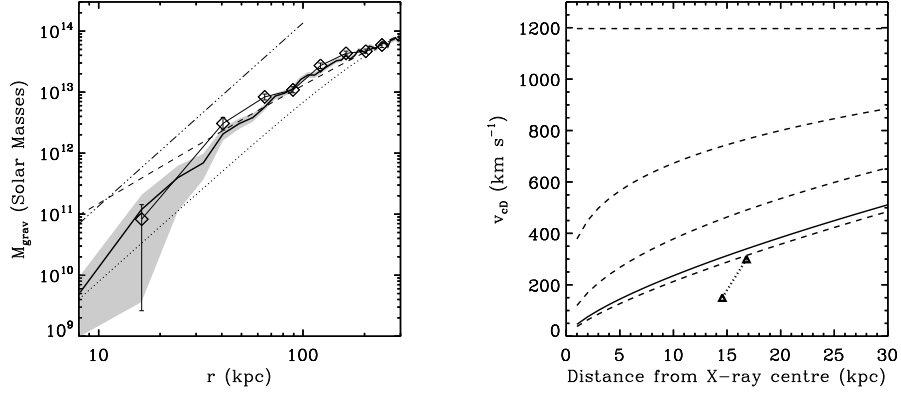


Figure 5. (Left panel) Gravitational mass profiles. The solid line is the mass profile obtained through the hydrostatic equilibrium equation applied to the results from the spatial deprojection on the gas temperature and density profiles. The diamonds are the total mass values obtained using the deprojected spectral temperature and density measurements. These values are compared with the best-fit results from ROSAT PSPC data (Ettori & Fabian 1999) using a β model (dotted line) and a gas density model in hydrostatic equilibrium with a Navarro, Frenk, & White (NFW, 1997) potential (dashed line). The three-dots-dash line indicates the upper limit from an assumed tidal shear in the H filament due to the central cluster potential. (Right panel) Predicted velocity of the CD galaxy under the effect of different gravitational potentials as a function of the separation from the X-ray centre assumed to be consistent with the deepest point of the potential well. The solid line indicates the estimated potential and the dashed lines are for dark matter density profiles with power law index of $\{0.5, \{1$ (as in NFW), $\{1.5$ and $\{2$ upwards, respectively. The dotted line shows the range of the values in the velocity-separation space for angles with respect the line-of-sight between 0 and 60 degrees (at 0, these values are 150 km s^{-1} and about 9 arcsec, respectively).

as $v_{cd} = (2GM_{grav}/r)^{0.5}$, where G is the gravitational constant and M_{grav} is the total gravitating mass within the radius r . Fixing the gravitational mass at $r=100 \text{ kpc}$, we can change the power law index and investigate the behaviour of the CD velocity. A CD velocity larger than 400 km s^{-1} is required for potential well described by a dark matter density profile steeper than r^{-1} . Given the observed velocity offset along the line of sight, the presence of a density profile flatter than a NFW profile is then required.

4.1. Cooling gas in A1795

The gas in the core of A1795 would cool radiatively in about 10^9 years (3.8×10^8 yrs in the central 10 kpc radius, with 10th and 90th percentile of 3.2 and 4.4×10^8 yrs, respectively), approaching the estimated age of the Universe at

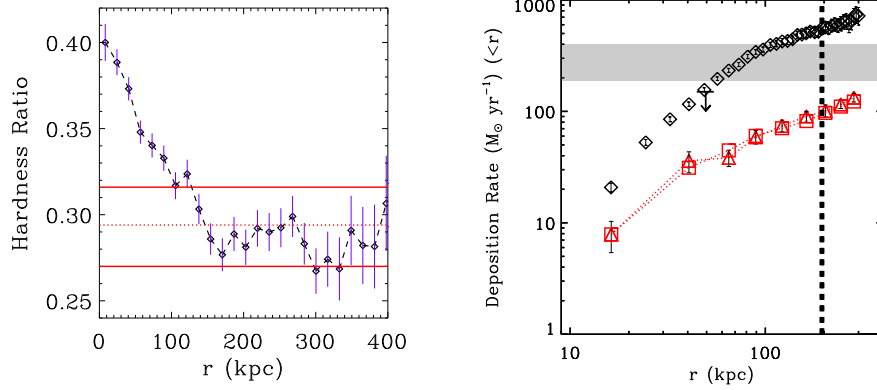


Figure 6. (Left) Ratio between counts with energy < 1.5 and > 1.5 keV. (Right) Spatial (diamonds) and spectral (triangles: from concentric rings; squares: from annuli) deprojection results on the integrated deposition rate, $\dot{M}(< r)$. The RGS-XMM upper limit is indicated by the downward arrow. The vertical dashed line corresponds to the radius of 191 kpc where $t_{\text{cool}} = t_{\text{H}_0}$. The dashed region shows the 90% confidence level from ASCA analysis (Allen et al. 2001). Note that a break at 100 kpc is present in both the two profiles and in the colour ratio profile.

the cluster redshift of 1.2×10^{10} years at about 200 kpc (Fig. 6). This can be considered as an upper limit on the region where strong cooling is taking place. In particular, the physical extension of the central region where a X-ray soft component dominates the emission can be obtained from the flattening at about 100 kpc of the X-ray colour profile shown in Fig. 6.

The deviation between the spatial and spectral results on the \dot{M} -profile, apart from the central 2 bins where the assumed spherical geometry is probably inappropriate given the observed cooling wake, is due to limitations on the validity of the steady-state cooling flow model. The dynamical scenario, in which cooling flows establish and evolve, considers merging with infalling substructures that interrupt the subsonic flow of material.

Recent analysis of Newton-XMM data of A1795 (Tamura et al. 2001) does not show detectable emission from gas cooling below 1.2 keV. Our lower limit from the deprojection of the best-fit gas temperature in the central 20 kpc radius is 1.8 keV at 90 per cent confidence level. When an isobaric cooling flow component is considered to model the Newton-XMM Reflection Grating Spectrometers (RGS) spectra of the central 30'' radius region, an upper limit (90% level of confidence) of $150 M_{\odot} \text{ yr}^{-1}$ is obtained (Tamura et al. 2001). This value is larger than our value of $43 M_{\odot} \text{ yr}^{-1}$ (90% limit of $56 M_{\odot} \text{ yr}^{-1}$) measured within the same region of 30 arcsec from the X-ray centre. The Chandra-determined cooling flow therefore appears to be consistent with the present Newton-XMM RGS constraint. Within the central 200 kpc, we estimate \dot{M} of about $100 M_{\odot} \text{ yr}^{-1}$ ($< 121 M_{\odot} \text{ yr}^{-1}$ at 90% c.l.). In the model that we adopt, the cool emission is suppressed with an intrinsic absorption of about $3 \times 10^{21} \text{ particle cm}^{-2}$. If we

use the same model that describes the RGS spectra, fixing the outer thermal component to 6.4 keV and the Galactic column density to $3 \times 10^{20} \text{ cm}^{-2}$, and not including any intrinsic absorption, we measure a normalization for the cooling flow component of $85 M_{\odot} \text{ yr}^{-1}$ (90% confidence limit range of $76\text{--}92 M_{\odot} \text{ yr}^{-1}$) but we obtain a considerably worse χ^2 . The intrinsic absorption can be interpreted as one method to suppress the line emission from gas below 1.5 keV. Other methods and related issues are discussed by Peterson et al. (2001) and Fabian et al. (2001a). More discussion on the deposition rate in A1795 is presented in Ettori et al. (2001).

5. The metals distribution in the cluster cores

The X-ray emitting plasma is about 5 times more luminous than the stars in galaxies and, thus, is the major reserve of both baryons and heavy metals contained in galaxy clusters, since the Iron abundance is typically between 0.3 and 0.5 times the solar value. Studies on the correlation between Fe mass and light coming from E and S0 galaxies (Amaud et al. 1992, Renzini 1997) conclude that larger amount of iron resides in the intracluster medium than inside galaxies and its enrichment originated through releases from early-type galaxies. The processes that preferably enrich the plasma are (i) (proto)galactic winds (De Young 1978), that occur at early times and are characterized from supernova (SN) type II ejecta with large abundance of elements, and (ii) ram pressure stripping (Gunn & Gott 1972), that takes place on longer time scales due to the continuous accretion of field galaxies in the cluster potential well and produces mostly SN Ia ejecta. What discriminates between these two main processes is the different elemental mass yields: SN Ia ejecta tend to be rich in Ni, whereas SN II ejecta present larger ratio between elements (e.g., O, Mg, Ar, Ca, S, Si) and Fe. Recent evidence of iron gradients in cluster cores with decreasing ratio between elements and Fe moving inward suggest that, while the global intracluster metal abundances are consistent with SN II ejecta (Mushotzky & Loewenstein 1997), SN Ia productions are dominant in the central cluster regions (e.g. Finoguenov, David & Ponman 2000, Dupke & Amaud 2001).

We have investigated the metals distribution in A1795. The radial profiles of the resolved element abundances and the fraction of SN Ia, $f_{\text{SN Ia}}$, responsible for those profiles are plotted in Fig. 7. The fraction in number of the SN Ia is above 60 per cent in the inner 200 kpc. The amount of the total iron produced in SN Ia is then $M_{\text{Fe,SN Ia}} = M_{\text{Fe}} \frac{1 + 3.5}{f_{\text{SN Ia}} - 1} (f_{\text{SN Ia}} - 1)^{-1} (0.12 = 0.74)$ in the central 200 kpc (here we assume a contribution of $0.74 M_{\odot}$ of iron from SN Type Ia, $0.12 M_{\odot}$ from SN Type II and a conversion factor of 3.5 between numbers of Type II and Type Ia). This star formation activity releases energy during supernova explosions providing an amount of thermal energy per gas particle, $E = 10^{51} N_{\text{SN II}} (\epsilon_p) = M_{\text{gas}}$, where 10^{51} erg is the kinetic energy released by one SN, (ϵ_p) is the efficiency of this kinetic energy in heating the ICM through galactic winds. When typical values for the inner part of A1795 are adopted, $E = 0.2 - 0.6 \text{ keV}$, i.e. only about 8 per cent of the thermal energy per particle measured (cf. Fig. 1).

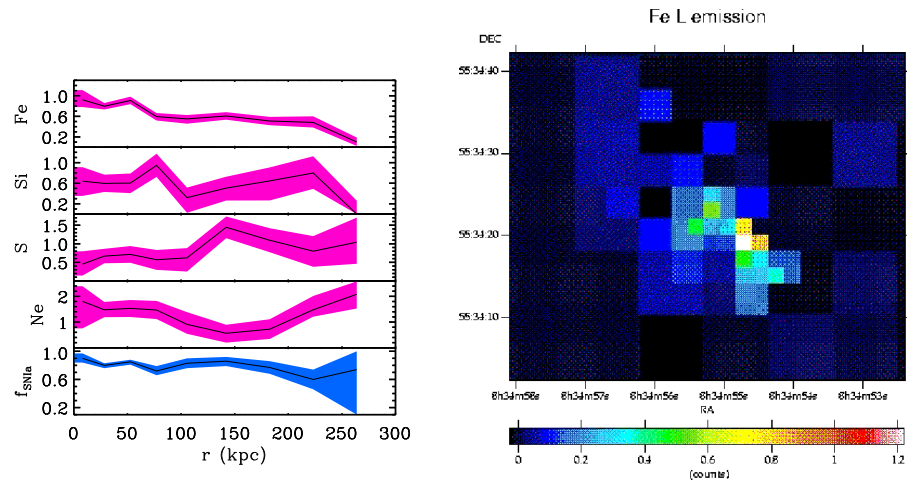


Figure 7. (Left) A1795 (Ettori et al. 2001): abundance respect to the solar value of Fe, Si, S, Ne as in Grevesse & Sauval (1998). The bottom panel provides the fraction of SN Ia that are expected to contribute to the enrichment of the intracluster medium. (Right) 4C+55.16 (Iwasawa et al. 2001): adaptively pixel-binned Chandra image of the continuum-subtracted Iron-L emission of the core of the cluster at redshift 0.24. The plume located at 3 arcsec to the South-West of the centre has a spectrum that requires a metal abundance larger than 2 solar (90% confidence level) and an abundance pattern typical of Supernovae Ia.

6. Conclusions

The Chandra observatory is providing measurements on arcsec scale (tens of kpc for nearby objects) of the plasma temperature and metals abundance with relative uncertainties of about 10 per cent.

The gas temperature profile raises with radius up to the cooling radius and then remains constant and equal to the virial value, T_{vir} , within few hundred kpc. Therefore, two temperatures, at least, are individuated in the cluster plasma, T_{vir} and $T_{\text{vir}}/3$ in the very central region. Sharp jumps in the temperature/density distributions are seen in many cluster cores, suggesting that the thermal conduction is suppressed and the ICM is inhomogeneous.

There is not evidence for gas cooling below 1–2 keV. If strong shocks in cores are responsible for heating the gas and stopping and/or reducing the cooling flow, then almost 10 per cent of the observed cooling flow clusters should show evidence of this activity (cf. David et al. 2001). No detection of strong shocks has been obtained up to now (cf. also the Perseus case). Peterson et al. (2001) and Fabian et al. (2001) discuss more in depth the problems concerning to the cooling flow scenario after Newton-XMM and Chandra observations.

Finally, the cores of cooling flow clusters show hints of a positive gradient within 20–40 kpc (see Glenn Morris's contribution in this volume) and negative outward in the azimuthally averaged radial distribution of the metals. However, strong azimuthal variations are observed (e.g. in the core of the cluster around

4C+55.16, Iwasawa et al. 2001; Fig. 7). SuperNovae type Ia appear to be dominant in the enrichment process of these regions.

References

- Allen S.W. et al. 2001, *MNRAS*, 322, 589
 Aumaud M. et al. 1992, *A & A*, 254, 49
 Binney, J., & Cowie, L.L., 1981, *ApJ*, 247, 464
 Cavaliere A. & Fusco-Femiano R., 1978, *A & A*, 70, 677
 Crawford C.S. et al. 1999, *MNRAS*, 306, 875
 Cowie L.L., & McKee C.F., 1977, *ApJ*, 211, 135
 David L.P. et al. 2001, *ApJ*, in press (astro-ph/0010224)
 De Young D., 1978, *ApJ*, 223, 47
 Dupke R.A. & Aumaud K.A., 2001, *ApJ*, 548, 141
 Ettori S., & Fabian A.C., 1999, *MNRAS*, 305, 834
 Ettori S., & Fabian A.C., 2000, *MNRAS*, 317, L57
 Ettori S. et al., 2001, *MNRAS*, submitted
 Fabian A.C., 1994, *ARAA*, 32, 277
 Fabian A.C. et al. 2000, *MNRAS*, 318, L65
 Fabian A.C. et al. 2001a, *MNRAS*, 321, L20
 Fabian A.C. et al. 2001b, *MNRAS*, 321, L33
 Finoguenov A., David L.P., Ponman T.J., 2000, *ApJ*, 544, 188
 Gervase N. & Sauval A.J. 1998, *Space Sci Rev.*, 85, 161
 Gunn J.E., & Gott III J.R., 1972, *ApJ*, 176, 1
 Hu E.M., Cowie L.L., & Wang Z., 1985, *ApJS*, 59, 447
 Iwasawa K. et al. 2001, *MNRAS*, in press (astro-ph/0110216)
 Markevitch M., 1996, *ApJ*, 465, L1
 Markevitch M. et al., 2000, *ApJ*, 541, 542
 Mazzotta P. et al., 2001, *ApJ*, in press (astro-ph/0102291)
 Mushotzky R.F., & Loewenstein M., 1997, *ApJ*, 481, L63
 Navarro J.F., Frenk C.S., & White S.D.M., 1997, *ApJ*, 490, 493
 Oegerle, W.R., & Hill, J.M., 1994, *AJ*, 107, 857
 Peres C.B. et al., 1998, *MNRAS*, 298, 416
 Peterson J.R. et al., 2001, *A & A*, 365, L104
 Renzini A. 1997, *ApJ*, 488, 35
 Sarazin, C.L., 1988, *X-ray emission from clusters of galaxies*, CUP
 Spitzer, L., 1962, *Physics of Fully Ionized Gases* J. Wiley & sons
 Tamura T. et al., 2001, *A & A*, 365, L87
 Vikhlinin A., Markevitch M., & Murray S.S. 2001, *ApJ*, 551, 160